

Accurate low-order modeling of electrified falling films at moderate Reynolds number

Alexander W. Wray*

Mathematics and Statistics, University of Strathclyde, Livingstone Tower, 26 Richmond Street, Glasgow, G1 1XH, United Kingdom

Omar K. Matar

Department of Chemical Engineering, Imperial College London, South Kensington Campus, SW7 2AZ, United Kingdom

Demetrios T. Papageorgiou

Department of Mathematics, Imperial College London, South Kensington Campus, SW7 2BZ, United Kingdom

(Received 4 October 2016; published 22 June 2017)

The two- and three-dimensional spatio-temporal dynamics of a falling, electrified leaky dielectric film are studied. The method of weighted residuals is used to derive high-order models that account for both inertia as well as second-order electrostatic effects. The models are validated against both linear theory and direct numerical simulations of the Navier-Stokes equations. It is shown that a simplified model offers a rapid computational option at the cost of a minimal decrease in accuracy. This model is then used to perform a parametric study in three dimensions.

DOI: [10.1103/PhysRevFluids.2.063701](https://doi.org/10.1103/PhysRevFluids.2.063701)

I. INTRODUCTION

Electrohydrodynamically driven flows have a wide variety of practical applications that stem from the ability to use an electric field to control the behavior of a fluid. For example, it is well known that the interfacial area of a film is closely linked to heat and mass transfer rates [1,2]. Enhancing these transfer rates is central to a range of engineering applications including falling film reactors and distillation columns [3,4]. Control strategies using electric fields also allow for patterning at the micro- and nanoscale in thin polymeric films, which can be used to create systems such as solar panels, fuel cell electrodes, micro-electronic devices, and self-cleaning surfaces [5–7]. This electric-fields-based control also finds applications in other situations involving a particulate phase (an example of this is the suppression of the so-called “coffee-stain effect” in evaporating sessile drops [8,9]).

Due to their relevance to industrial applications, it is no surprise that electrohydrodynamic (and the closely related magnetohydrodynamic) flows have been investigated quite extensively experimentally, starting with Gilbert’s 1600 work *De Magnete*. Early work on electrohydrodynamics primarily focused on perfect conductors and perfect dielectrics [10], but this changed with the work of Allan and Mason [11], who began to study leaky dielectrics: poorly conducting fluids. In order to study such leaky dielectrics, we will use the most common model applied in the literature, the Taylor-Melcher leaky dielectric model.

In planar geometries extensive investigations have been carried out both in linear [12] and nonlinear [13–16] regimes. This has included work on the full leaky dielectric formulation [17,18] as well as the simpler situations where both regions have large conductivities [19], or indeed where one region is a perfect conductor [20]. Notably, given a permittivity ratio ϵ_R and a conductivity ratio

*alexander.wray@strath.ac.uk

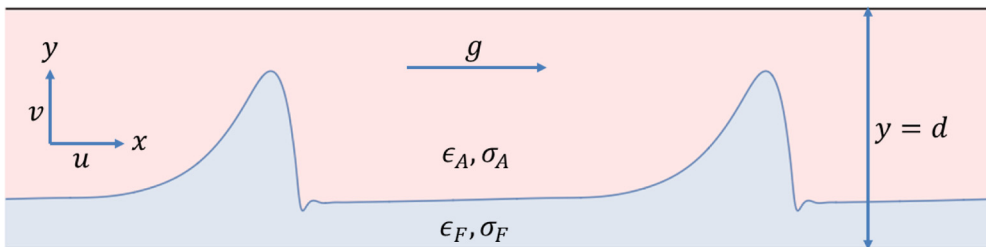


FIG. 1. Schematic representation of the flow showing a film flowing vertically down, subjected to an electric field imposed across electrodes separated by a distance d .

σ_R between the two regions, the two dimensionless groupings $(1 - \sigma_R/\epsilon_R)$ and $(1 - \sigma_R^2/\epsilon_R)$ have previously been shown to be critical to determining whether the electric field is linearly stabilizing or destabilizing [19,21]. In the present work, we will derive low-order models for electrified films by assuming that the characteristic length of a wave is large relative to the film thickness: the long-wave approximation; this allows a dramatic simplification of the Navier-Stokes equations. One option is to solve order-by-order to eliminate the cross-stream co-ordinate [20]; this technique is referred to here as the *gradient expansion* approach [22]. However, in the presence of inertia such an expansion is known to produce an unphysical “blowup” phenomenon [23,24] even when capillarity is incorporated: the interfacial thickness can become infinite in finite time. In order to resolve this blowup, a variety of approaches have been suggested, including a *Padé approximant*-based regularization of the Benney equation [25] or the application of the Kármán-Polhausen technique to the leading-order contributions to the long-wave equations. However, all such approaches have been found to be lacking in accuracy [26], especially far from instability threshold.

The method of weighted residuals [27] has resolved the aforementioned shortcomings. The technique is essentially a separation of variables approach together with an elegant weighting selection during the computation of the requisite residuals (and, indeed, this has been shown to be optimal in a certain sense [27,28]). The method results in a coupled system of four partial differential equations for the height, flux, and two subsidiary fields which measure the departure of the streamwise velocity profile from the parabolic Nusselt one. The model, even when extended to three dimensions [22], leads to no unphysical blowup, and the results of direct numerical simulations are well matched even into regimes where inertia becomes significant (i.e., the so-called “drag-inertia” regime [22]). The model itself is lengthy, but Scheid *et al.* [22] demonstrate an alternative method by a *Padé* regularization technique that retains the second-order accuracy exhibited by the full model, while still only requiring two coupled equations, albeit at the expense of accuracy at higher values of the Reynolds number [29]. We show here that the method of weighted residuals may be extended to be used for long-wave models incorporating electric fields, with a resultant increase in accuracy.

The rest of this paper is organized as follows. We begin by giving the governing equations in Sec. II. We then reduce the governing equations to a low-order nonlinear model by use of the long-wave approximation together with the method of weighted residuals in Sec. III. The two-dimensional version of the model is validated via comparison against full linear theory and direct numerical simulations of the Navier-Stokes equations in Sec. IV. The model is simulated in three dimensions to perform a large-scale parametric study in Sec. V. Finally, we provide our conclusions in Sec. VI.

II. PROBLEM FORMULATION

We consider a film flowing down a vertical electrode, bounded by an inviscid gas phase and a parallel electrode, as shown in Fig. 1. An electric field is induced in both phases due to a voltage difference across the electrodes, which are held at a fixed distance d . The problem is governed by the Navier-Stokes equations for the hydrodynamics, together with Laplace’s equation for the potential fields, complemented by appropriate boundary conditions [17,30]. We nondimensionalize

according to

$$\mathbf{u} = V\hat{\mathbf{u}}, \quad \mathbf{x} = H\hat{\mathbf{x}}, \quad p = \frac{V\mu}{H}\hat{p}, \quad t = \frac{H}{V}\hat{t}, \quad q = \frac{\epsilon_0\phi_b}{H}\hat{q}, \quad \phi = \phi_b\hat{\phi}, \quad (1)$$

where $\mathbf{x} = (x, y)$ are the usual Cartesian coordinates with x directed down the film-bounding electrode and y normal to it; $\mathbf{u} = (u, v)$ is the velocity vector in the fluid, p is the pressure, t is time, q is the local charge accumulation on the interface; $\phi_{A,F}$ are the potential fields in the liquid and gas regions respectively; H is the undisturbed film thickness; μ is the viscosity of the fluid; $V = \rho g H^2 / \mu$ is a characteristic velocity with ρ the (constant) density of the fluid; ϵ_0 is the permittivity of free space; ϕ_b is the (constant) potential of the outer electrode (with the potential at the inner electrode held at $\phi_F = 0$ without loss of generality). The usual dimensionless relative permittivities of the liquid and gas regions are given respectively by ϵ_F and ϵ_A . For the moment we work purely in two dimensions, neglecting the z direction.

We now suppress the hat decoration. The equations describing the system are as described by Craster and Matar [17] and references therein. The dimensionless Navier-Stokes equations are given by

$$\text{Re}(u_t + uu_x + vu_y) = 1 - p_x + u_{xx} + u_{yy}, \quad (2)$$

$$\text{Re}(v_t + uv_x + vv_y) = -p_y + v_{xx} + v_{yy}, \quad (3)$$

$$u_x + v_y = 0, \quad (4)$$

where $\text{Re} = \frac{\rho V H}{\mu}$ is the Reynolds number, subject to the normal and tangential stress conditions at the interface, $y = h$, respectively given by

$$\begin{aligned} (1 + h_x^2) \left(p - \frac{\kappa}{\text{Ca}} \right) &= \frac{2}{1 + h_x^2} [v_y + h_x^2 u_x - h_x(v_x + u_y)] \\ &\quad - E_b \left[\frac{1}{2} (\phi_x^2 - \phi_y^2) (h_x^2 - 1) - 2h_x \phi_x \phi_y \right]_F^A, \end{aligned} \quad (5)$$

$$(1 - h_x^2)(u_y + v_x) + 2h_x(v_y - u_x) = -E_b(1 + h_x^2)^{1/2}(\phi_x + h_x\phi_y)q, \quad (6)$$

where $\text{Ca} = V\mu/\gamma$ and $E_b = \frac{\epsilon_0\phi_b^2}{\mu V}$ are the hydrodynamic capillary number and dimensionless electric field strength, governing the relative significance of viscosity to surface tension, and electrostatic effects, respectively, $\kappa = -h_{xx}/(1 + h_x^2)^{3/2}$ is the curvature, and $[\cdot]_F^A$ represents the jump in the quantity across the interface.

The potentials are governed by Laplace's equation

$$\phi_{A,F,xx} + \phi_{A,F,yy} = 0 \quad (7)$$

subject to the equipotentials at the upper and lower electrodes,

$$\phi_F|_0 = 0, \quad \phi_A|_d = 1, \quad (8)$$

the appropriate interfacial conditions evaluated at $y = h$: continuity of potential,

$$\phi_F = \phi_A, \quad (9)$$

the Gauss condition,

$$-q = [\epsilon_{A,F}(\phi_y - h_x\phi_x)]_F^A, \quad (10)$$

and the surface charge evolution equation,

$$\begin{aligned} (1 + h_x^2)q_t + (u + vh_x)q_x - q(h_x^2u_x - h_xu_y - h_xv_x + v_y) \\ = (1 + h_x^2)^{1/2}[\Sigma_{A,F}(\phi_{Ay} - h_x\phi_{Ax})]_F^A, \end{aligned} \quad (11)$$

where $\Sigma_{A,F} = \sigma_{A,F} H / \epsilon_0 \phi_b V$ are the dimensionless conductivities of the liquid and gas regions respectively, and $\cdot|_{y_0}$ represents evaluation of the respective quantity at the position $y = y_0$. Finally, the kinematic equation is imposed at $y = h$:

$$h_t + u h_x = v \quad \text{or} \quad h_t + f_x = 0, \quad (12)$$

where $f = \int_0^h u dy$ is the streamwise flux.

The system supports a steady, basic solution, denoted by overbars, with no x variation, $v = \bar{v} = 0$, $h = \bar{h} = 1$. The electrostatic problem is governed by

$$\phi_{A,F,yy} = 0, \quad \phi_F|_0 = 0, \quad \phi_A|_d = 1, \quad \phi_F|_1 = \phi_A|_1, \quad \Sigma_F \phi_{F,y}|_1 = \Sigma_A \phi_{A,y}|_1,$$

giving

$$\bar{\phi}_F = \frac{\Sigma_A y}{\Sigma_A - \Sigma_F(1-d)}, \quad \bar{\phi}_A = \frac{\Sigma_A + \Sigma_F(y-1)}{\Sigma_A - \Sigma_F(d-1)} \Rightarrow -\bar{q} = \frac{\epsilon_A \Sigma_F - \epsilon_F \Sigma_A}{\Sigma_A + \Sigma_F(d-1)}.$$

The streamwise velocity u satisfies

$$u_{yy} = 1, \quad u_y|_1 = 0, \quad u|_0 = 0 \Rightarrow u = y - \frac{y^2}{2}.$$

III. LONG-WAVE MODELING

We begin by deriving the electrostatically modified boundary layer equations. The long-wave substitution $x = \epsilon^{-1} \tilde{x}$ is applied and balancing terms in the kinematic condition (12) suggests making the additional substitutions $t = \epsilon^{-1} \tilde{t}$ and $v = \epsilon \tilde{v}$. Dropping the tilde decorations, the Navier-Stokes equations become

$$\text{Re}(\epsilon u_t + \epsilon u u_x + \epsilon v u_y) = -\epsilon p_x + \epsilon^2 u_{xx} + u_{yy} + 1, \quad (13)$$

$$\text{Re}(\epsilon^2 v_t + \epsilon^2 u v_x + \epsilon^2 v v_y) = -p_y + \epsilon^3 v_{xx} + \epsilon v_{yy}, \quad (14)$$

$$u_x + v_y = 0. \quad (15)$$

The normal stress condition becomes

$$(1 + \epsilon^2 h_x^2) \left(p + \frac{\epsilon^2 h_{xx}}{\text{Ca}} \right) = \frac{2}{1 + \epsilon^2 h_x^2} [\epsilon v_y + \epsilon^3 h_x^2 u_x - \epsilon h_x (u_y + \epsilon^2 v_x)] + E_b \left\{ \epsilon_{A,F} \left[\frac{1}{2} (\epsilon^2 \phi_x^2 - \phi_y^2) (-1 + \epsilon^2 h_x^2) - 2 \epsilon^2 h_x \phi_x \phi_y \right] \right\}_F^A. \quad (16)$$

The tangential stress condition is given by

$$(\epsilon^2 h_x^2 - 1)(u_y + \epsilon^2 v_x) + 2 \epsilon^2 h_x (u_x - v_y) = \epsilon E_b (1 + \epsilon^2 h_x^2)^{1/2} (\phi_x + h_x \phi_y) q; \quad (17)$$

this may be reduced to

$$u_y = -\epsilon E_b E^T + \epsilon^2 [4 h_x u_x - v_x] + O(\epsilon^3), \quad (18)$$

where

$$E^T = (\phi_x + h_x \phi_y) q. \quad (19)$$

The charge evolution equation (11) rescales to give

$$\epsilon [q_t + (u|_h q)_x] + \epsilon^2 h_x [\Sigma_A \phi_{A,x} - \Sigma_F \phi_{F,x}] = \Sigma_A \phi_{A,y} - \Sigma_F \phi_{F,y}. \quad (20)$$

In order to produce a boundary-layer equation from (13) that is accurate at second order, we need an expression for p which is correct up to first-order. We assume that $\text{Ca} = O(\epsilon^2)$, so we make the

TABLE I. List of all models used.

Model name	Governing equations	Linearized form
Full model	(2)–(12)	(77)–(84)
Regularized, first-order electrostatics	(36), (75), (29), (30)	(85), (86)
Regularized, second-order electrostatics	(36), (75), (23), (32)–(34)	Appendix A
Simplified, first-order electrostatics	(36), (76), (29), (30)	
Simplified, second-order electrostatics	(36), (76), (23), (32)–(34)	

substitution $\text{Ca} = \epsilon^2 \widetilde{\text{Ca}}$ with $\widetilde{\text{Ca}} = O(1)$ [although we note that as the models are second-order, the capillary terms would be retained for $\widetilde{\text{Ca}}$ as large as $O(\epsilon^{-1})$]. We assume $E_b = O(1)$. We truncate (14) at first order and drop the tilde decoration to give

$$p_y = \epsilon v_{yy} + O(\epsilon^2). \quad (21)$$

This is integrated from y to h subject to (16), truncated at first order, given by

$$p|_h = -\frac{h_{xx}}{\text{Ca}} + E_b E^N + 2\epsilon(v_y - h_x u_y)|_h + O(\epsilon^2), \quad (22)$$

where

$$E^N = \left\{ \epsilon_{A,F} \left[\frac{1}{2} (1 - \epsilon^2 h_x^2) (\phi_y^2 - \epsilon^2 \phi_x^2) - \epsilon^2 2h_x \phi_x \phi_y \right] \right\}_F^A. \quad (23)$$

This gives

$$p(y) = -\frac{h_{xx}}{\text{Ca}} + E_b E^N - \epsilon(u_x + u_x|_h) + O(\epsilon^2), \quad (24)$$

where we have made use of the continuity equation as well as the fact that $u_y|_h = O(\epsilon)$. Substituting (24) into (13) gives

$$\epsilon \text{Re}(u_t + uu_x + vu_y) = u_{yy} + 2\epsilon^2 u_{xx} + 1 + \epsilon \frac{h_{xxx}}{\text{Ca}} + \epsilon E_x^N + \epsilon^2 \partial_x(u_x|_h) + O(\epsilon^3). \quad (25)$$

This is complemented by no-slip and no-penetration, the kinematic equation (12), and the tangential stress equation (18). Equations (25) and (18) are now solved by use of the method of weighted residuals. We begin by solving the electrostatic part of the problem in Sec. III A. We then solve the hydrodynamic part of the problem in Sec. III B. A summary of all the models is given in Table I.

A. Electrostatics

We will solve for the electrostatic potentials up to second-order using a separation of variables approach in line with the method of weighted residuals. We will see in Sec. IV A 4 that it is suitable to take the high conductivity limit, neglecting the left-hand side of the charge evolution equation (20). As a result the computed model will not contain an additional evolution equation for the charge. Then the potentials satisfy

$$\phi_{A,Fyy} + \epsilon^2 \phi_{A,Fxx} = 0, \quad \phi_F|_0 = 0, \quad \phi_A|_d = 1, \quad \phi_F|_h = \phi_A|_h, \quad (26)$$

$$\left(\phi_{Ay} - \epsilon^2 h_x \phi_{Ax} \right)|_h = \sigma_R \left(\phi_{Fy} - \epsilon^2 h_x \phi_{Fx} \right)|_h, \quad (27)$$

where $\sigma_R = \Sigma_F / \Sigma_A = \sigma_F / \sigma_A$ is the conductivity ratio. To leading order, this gives

$$\phi_{A,Fyy} = 0, \quad \phi_F|_0 = 0, \quad \phi_A|_d = 1, \quad \phi_{Ay}|_h = \sigma_R \phi_{Fy}|_h, \quad \phi_A|_h = \phi_F|_h, \quad (28)$$

whose solution is given by $\phi_F = c_F y$ and $\phi_A = 1 + c_A(y - d)$ where

$$c_A = \frac{\sigma_R}{h - \sigma_R(h - d)}, \quad c_F = \frac{1}{h - \sigma_R(h - d)}. \quad (29)$$

Then the functions E^N and E^T are given by

$$E^N = \frac{1}{2}(\epsilon_A c_A^2 - \epsilon_F c_F^2) + O(\epsilon^2), \quad E^T = (\epsilon_F c_F - \epsilon_A c_A)(c_F h)_x + O(\epsilon^2). \quad (30)$$

As we only need E^N and E^T correct to $O(\epsilon)$ for a second-order calculation for h alone (and not $\phi_{A,F}$), this is, in fact, sufficient. However, we are interested in retaining second-order accuracy for the electric fields. So we pose

$$\phi_F = c_F y + \epsilon^2 d_F y^3, \quad \phi_A = 1 + c_A(y - d) + \epsilon^2 d_A(y - d)^3, \quad (31)$$

where the polynomials have been selected to satisfy the equipotentials at the inner and outer electrodes. Mandating that Laplace's equation be satisfied up to $O(\epsilon^2)$, we find that $\frac{c_{A,F,xx}}{6} + d_{A,F} = 0$. Then the continuity of potential and current at the interface become two ODEs defining the electric fields up to second order, respectively,

$$c_F h - \epsilon^2 \frac{c_{F,xx}}{6} h^3 = 1 + c_A(h - d) - \epsilon^2 \frac{c_{A,xx}}{6} (h - d)^3, \quad (32)$$

$$\sigma_R \left[c_F - \frac{1}{2}(c_{F,x} h^2)_x \right] = c_A - \frac{1}{2}[c_{A,x}(h - d)^2]_x. \quad (33)$$

We now use the full second-order expression for E^T given by

$$E^T = [\epsilon_F(\phi_{F,y} - \epsilon^2 h_x \phi_{F,x}) - \epsilon_A(\phi_{A,y} - \epsilon^2 h_x \phi_{A,x})][\phi_F|_h]_x. \quad (34)$$

We also use the full expression (23) for E_x^N . This technically contains the term $[\epsilon_{A,F} \epsilon^4 h_x^2 \phi_x^2]_F^A$, which is formally of higher order than the rest of the terms. However, keeping the term actually affords for a more compact expression for E^N and improves accuracy at negligible computational cost, and so we retain it.

B. Hydrodynamics

1. Leading-order model

At leading order, the model is governed by

$$u_{yy} + 1 = 0 + O(\epsilon), \quad (35)$$

$$h_t + f_x = 0, \quad (36)$$

where we have assumed that $\text{Re} = O(1)$, so that $\epsilon \text{Re} \ll 1$. This is subject to the no-slip condition, and the leading-order of (18), $u_y|_h = 0$. This gives $u = (hy - y^2/2)$ to leading order so that the evolution equation is given by

$$h_t = -(h^3/3)_x + O(\epsilon). \quad (37)$$

2. First-order model

At first order, the problem is expressed by

$$\epsilon \text{Re}(u_t + uu_x + vu_y) = u_{yy} + 1 + \epsilon \left[\frac{h_{xxx}}{\text{Ca}} + E_b E_x^N \right], \quad (38)$$

subject to the no-slip boundary condition, as well as the tangential stress condition (18) curtailed at first order, given respectively by

$$u|_0 = 0, \quad u_y|_h = -\epsilon E_b E^T. \quad (39)$$

Thus we must solve for u , using the knowledge that, by continuity, $v = -\int_0^h u_x dy$. The basic idea is to expand u on a set of test functions. To simplify the problem we use the reduced coordinate $\hat{y} = y/h(x,t)$ to transform the problem from one on the interval $[0,h]$ to one on the interval $[0,1]$. To satisfy the Dirichlet condition at the wall, we posit that

$$u(x,y,t) = a_0(x,t)f_0(\hat{y}) + \epsilon \sum_{j=1}^N a_j(x,t)f_j(\hat{y}), \quad (40)$$

with $f_j(0) = 0 \forall j$. In particular, we select the polynomials as our test functions with $f_0(\hat{y}) = \hat{y} - \hat{y}^2/2$ [so that the leading-order solution is $u = h^2 f_0(\hat{y})$] and $f_j(y) = y^{j+1}$ for $j \geq 1$.

This gives us $N + 1$ unknowns: a_0, \dots, a_N . To solve this we can now simply substitute the candidate solution (40) into the momentum equation (38) and, with the help of boundary conditions (39), cancel polynomials to find an evolution equation relating a_0 and h , eliminating all other variables. This is complemented by the kinematic condition (36) and calculation of an explicit relation between f and a_0 :

$$f = \int_0^h u dy = a_0 h \int_0^1 (\hat{y} - \hat{y}^2/2) d\hat{y} + \epsilon h \sum_{j=1}^N a_j(x,t) \int_0^1 f_j(\hat{y}) d\hat{y} \quad (41)$$

$$= \frac{a_0 h}{3} + \epsilon \sum_{j=1}^N \frac{a_j h}{j+2}. \quad (42)$$

This gives a solution that shall be used shortly for validation. However, at second order this procedure is laborious, and so it shall be necessary to use the method of weighted residuals; we therefore illustrate this now. We integrate the momentum equation (38), curtailed at first order, with respect to y using a weighted average, with weight functions $w_j(y)$, to obtain residuals

$$\mathcal{R}_j = \int_0^h w_j(\hat{y}) \left[\epsilon \operatorname{Re}(u_t + uu_x + vu_y) - u_{yy} - 1 - \epsilon \frac{h_{xxx}}{\operatorname{Ca}} - \epsilon E_b E_x^N \right] dy. \quad (43)$$

These now form solvability conditions: setting $\mathcal{R}_j = 0 \forall j$ produces the requisite evolution equations. As explained by Ruyer-Quil and Manneville [28] and Ruyer-Quil *et al.* [31] any weighting scheme will converge towards the same equation given sufficient residuals. However, here we proceed explicitly as a judicious choice of weighting functions can greatly simplify the calculations to be performed.

We first notice that, for the model to be consistent at $O(\epsilon)$, all x and t derivatives of a_j may clearly be ignored for $j \geq 1$. Therefore, writing the residuals as

$$\int_0^h w_j(\hat{y}) [\epsilon \operatorname{Re}(u_t + uu_x + uu_y) - u_{yy}] dy = \left[1 + \epsilon \frac{h_{xxx}}{\operatorname{Ca}} + \epsilon E_b E_x^N \right] \int_0^1 w_j(\hat{y}) d\hat{y}, \quad (44)$$

it is clear that at leading order, the degree of the inertial terms is at most 4 (due to products and derivatives of $a_0 f_0$). Other terms may enter only via the term u_{yy} indicating that it is sufficient to introduce monomials up to degree 6, so that $N = 5$. To further simplify matters, consider this term a little more closely: double integration by parts gives

$$\int_0^h w_j\left(\frac{y}{h}\right) u_{yy} dy = \left[u_y w_j\left(\frac{y}{h}\right) \right]_0^h - \frac{1}{h} \left[u w_j'\left(\frac{y}{h}\right) \right] + \frac{1}{h^2} \int_0^h u w_j''\left(\frac{y}{h}\right) dy. \quad (45)$$

Consider this for the case $j = 0$: as $u|_0 = 0$, $\int_0^h u \, dy = f$ and $u_y|_h = -\epsilon E_b E^T$, this is independent of a_j for $j > 0$ under the conditions

$$w_0(0) = 0, \quad w_0'(1) = 0, \quad w_0'' = \text{const.} \quad (46)$$

This suggests taking $w_0'' = -1$ so that $w_0(\hat{y}) = \hat{y} - \hat{y}^2/2$. As noted elsewhere, this means that the optimal choice is to take the first weight function to be the first test function, i.e., exactly the Galerkin method, reflecting the fact that the friction operator ∂_{yy} is self-adjoint under the requisite boundary conditions. Thus, it suffices to compute only the first residual \mathcal{R}_0 as it does not contain terms involving a_j for $j \geq 1$, giving

$$\text{Re } f_i = \text{Re} \left(\frac{17}{7} \frac{f}{h} f_x + \frac{9}{7} \frac{f^2}{h^2} h_x \right) + \frac{5}{6} h - \frac{5}{2} \frac{f}{h^2} + \frac{5}{6} \frac{h}{\text{Ca}} h_{xxx} + E_b \left[-\frac{5}{4} E^T + \frac{5}{6} h E_x^N \right]. \quad (47)$$

3. Second-order model

In order to extend the model to incorporate all second-order terms, we follow a multistep process. First, we determine how many independent fields are required to prescribe u at first order. This is then used to write u in its simplest form, and thereby to pose an appropriate second-order form for u . A judicious choice of weighting polynomials is then used again to determine evolution equations for the required fields. So we begin by evaluating explicit expressions for the a_j , $1 \leq j \leq 5$. This is done by substitution of (40) into (38) and cancellation of polynomials, giving

$$a_1 = -\frac{E_b}{2} h E^T - \frac{1}{2} \text{Re } h f_i - \frac{3}{5} h \text{Re } \partial_x \left(\frac{f^2}{h} \right), \quad (48)$$

$$a_2 = \text{Re} \left(\frac{1}{2} h f_i + f f_x \right), \quad a_3 = -\frac{1}{8} f_i h - \frac{3}{4} \frac{f^2}{h} h_x, \quad (49)$$

$$a_4 = -\frac{3}{40} \text{Re } h^6 \partial_x \left(\frac{f^2}{h^6} \right), \quad a_5 = \frac{\text{Re}}{80} h^6 \partial_x \left(\frac{f^2}{h^6} \right). \quad (50)$$

Now, $a_4 = -6a_5$, $a_2 = -4a_3 + 40a_5$ and $a_1 = 4a_3 - 48a_5 + E_b h E^T/2$. By (42), it is seen that

$$a_0 = \frac{3f}{h} - \left[-\frac{E_b}{2} h E^T + \frac{8}{5} a_3 - \frac{144}{7} a_5 \right]. \quad (51)$$

Thus u may be seen to be

$$u = \frac{3f}{h} f_0(\hat{y}) + E_b h E^T \tilde{f}_1(\hat{y}) + a_3 \tilde{f}_3(\hat{y}) + a_5 \tilde{f}_5(\hat{y}), \quad (52)$$

where $\tilde{f}_1 = \frac{3}{4} \hat{y}^2 - \frac{1}{2} \hat{y}$, $\tilde{f}_3 = \hat{y}^4 - 4\hat{y}^3 + \frac{24}{5} \hat{y}^2 - \frac{8}{5} \hat{y}$, and $\tilde{f}_5 = \hat{y}^6 - 6\hat{y}^5 + 40\hat{y}^3 - \frac{408}{7} \hat{y}^2 + \frac{144}{7} \hat{y}$. Thus, where naïvely it might be expected that u requires six fields to prescribe it, we can see that in fact only four are required: $f/h, a_3, a_5$, and hE^T . For the purposes of the weighted residual method, it is best to proceed to an orthogonalized set of polynomials. With this in mind, a set of three orthogonal polynomials are constructed from $f_0, \tilde{f}_1, \tilde{f}_3$, and \tilde{f}_5 , normalized so that the coefficient of \hat{y} in each instance is unity. To complete the set, an additional polynomial including the contribution of \tilde{f}_1 is incorporated to give the same polynomials as in Ruyer-Quil *et al.* [31]:

$$F_0(\hat{y}) = \hat{y} - \frac{\hat{y}^2}{2}, \quad (53)$$

$$F_1(\hat{y}) = \hat{y} + \frac{17}{6} \hat{y}^2 + \frac{7}{3} \frac{\hat{y}^3}{12} \hat{y}^4, \quad (54)$$

$$F_2(\hat{y}) = \hat{y} - \frac{13}{2} \hat{y}^2 + \frac{57}{4} \hat{y}^3 - \frac{111}{8} \hat{y}^4 + \frac{99}{16} \hat{y}^5 - \frac{33}{32} \hat{y}^6, \quad (55)$$

$$F_3(\hat{y}) = \hat{y} - \frac{531}{62} \hat{y}^2 + \frac{2871}{124} \hat{y}^3 - \frac{6369}{248} \hat{y}^4 + \frac{29601}{2480} \hat{y}^5 - \frac{9867}{4960} \hat{y}^6. \quad (56)$$

With respect to this basis, u may be expanded as

$$u = \frac{3}{h}[f - \epsilon(s_1 - s_2 - s_3)]F_0(\hat{y}) + 45\epsilon\frac{s_1}{h}F_1(\hat{y}) + 210\epsilon\frac{s_2}{h}F_2(\hat{y}) + 434\epsilon\frac{s_3}{h}F_3(\hat{y}), \quad (57)$$

formed such that the relation $f = \int_0^h u \, dy$ is preserved.

Next, the new value of N must be determined. Consideration of the inertial terms suggests that additional orthogonal polynomials up to degree 10 ($N = 9$) are required. Thus, u may be expanded as

$$u = \frac{3}{h} \left(f - \epsilon \sum_{j=1}^3 s_j - \epsilon^2 \sum_{j=4}^9 c_j s_j \right) F_0(\hat{y}) + 45\epsilon\frac{s_1}{h}F_1(\hat{y}) + 210\epsilon\frac{s_2}{h}F_2(\hat{y}) \\ + \frac{434}{h}\epsilon \left[s_3 - \epsilon \sum_{j=4}^9 d_j s_j(x,t) \right] F_j(\hat{y}) + \epsilon^2 \sum_{j=4}^9 \frac{s_j}{h} F_j(\hat{y}). \quad (58)$$

It turns out that neither the constants c_j , d_j nor the values of the s_j for $4 \leq j \leq 9$ need ever be calculated explicitly. First, it is clear that given values of d_j , the values of c_j may be selected so that $\int_0^h u \, dy = f$. The values of d_j shall be selected shortly, in such a way that the weighted residual procedure need never calculate the values of the s_j .

The set $F_i, 0 \leq i \leq 3$ is closed with respect to the operations required in evaluating the residuals. Thus, by prescribed orthogonality, no additional polynomials are required. Therefore the residuals

$$\mathcal{R}_j = \int_0^1 F_j(\hat{y}) \left\{ \epsilon \operatorname{Re}(u_t + uu_x + wu_y) - u_{yy} - 2\epsilon^2 u_{zz} \right. \quad (59)$$

$$\left. - 1 - \epsilon \left[\frac{h_{xxx}}{\operatorname{Ca}} + E_b E_x^N \right] - \epsilon^2 \partial_x(u_x|_h) \right\} \quad (60)$$

may be evaluated for $0 \leq j \leq 3$. This is complemented by the full second-order tangential stress condition (18).

The only term by which the s_j , $4 \leq j \leq 9$ may enter is the u_{yy} . So let us calculate explicitly:

$$\int_0^h F_j(y/h) u_{yy} \, dy \quad (61)$$

$$= [F_j(y/h) u_y]_0^h - \left[\frac{F_j'(y/h) u}{h} \right]_0^h + \int_0^h \frac{F_j''(y/h) u}{h^2} \, dy \quad (62)$$

$$= F_j(1) u_y(h) - \delta_{3j} \frac{F_3'(1) u(h)}{h} + \frac{F_j''(0) f}{h^2} + \int_0^h \frac{[F_j''(y/h) - F_j''(0)] u}{h^2} \, dy. \quad (63)$$

Now, $u|_0 = F_j(0) = F_0(1) = F_1(1) = F_2(1) = 0$. Using the tangential stress condition to evaluate the first term on the final line, the terms d_j and s_j for $4 \leq j \leq 9$ may now only enter via the term $\delta_{3j} \frac{F_3'(1) u(h)}{h}$, for $j = 3$. Therefore, we select the d_j so that the coefficient of s_j is 0 in Eq. (58) when $y = h$ (note that this is of course a constant independent of h , as required).

Explicit computation using symbolic algebra gives the full second-order model, comprising evolution equations for each of h , f , s_1 , s_2 , and s_3 . This full model is rather lengthy and may be inferred from Ref. [32]. Hence, we do not state it here, and instead seek a reduced model.

4. Reduced model

In the evolution equation for f , terms involving s_1 , s_2 , and s_3 only appear at $O(\epsilon)$ and higher. Therefore, we seek explicit expressions for s_1 , s_2 , and s_3 in terms of h and f and their derivatives.

This is done by curtailing the evolution equations for s_1 , s_2 , and s_3 at $O(\epsilon)$ and solving:

$$s_1 = \frac{1}{40} E_b h^2 E^T + \text{Re} \frac{1}{210} h^2 f_t + \text{Re} \frac{74}{5775} f h f_x - \text{Re} \frac{19}{1925} f^2 h_x, \quad (64)$$

$$s_2 = -\frac{299}{53760} E_b h^2 E^T - \text{Re} \frac{2}{17325} h f_x + \text{Re} \frac{2}{5775} f^2 h_x, \quad (65)$$

$$s_3 = \frac{5}{3584} E_b h^2 E^T. \quad (66)$$

These may now be substituted into residual \mathcal{R}_0 to obtain the simplified model:

$$\begin{aligned} h_t &= -f_x, \quad (67) \\ \epsilon \text{Re} f_t &= \frac{5}{6} h - \frac{5}{2} \frac{f}{h^2} - \epsilon \text{Re} \frac{17}{7} \frac{f}{h} f_x + \epsilon \text{Re} \frac{9}{7} \frac{f^2}{h^2} h_x - \epsilon^2 \frac{9}{2h} f_x h_x \\ &\quad + \epsilon^2 4 \frac{f}{h^2} h_x^2 + \epsilon^2 \frac{9}{2} f_{xx} - \epsilon^2 6 \frac{f}{h} h_{xx} + \epsilon \frac{5}{6} \frac{h_{xxx} h}{\text{Ca}} \\ &\quad + \epsilon \frac{5}{6} E_b h E_x^N - \epsilon \frac{5}{4} E_b E^T + \text{Ine}[h, f] + \text{Ele}[h, f, E^T], \quad (68) \end{aligned}$$

where the terms $\text{Ine}[h, f]$ and $\text{Ele}[h, f, E^T]$ are complicated second-order terms accounting for the effects of inertia and electrostatics respectively. By the use of leading-order equivalences such as $f = h^3/3$, the former may be reduced to $\text{Ine}[h, f] = -\frac{\epsilon^2 \text{Re}}{630} h^7 h_x^2$ [22]. The latter is given by

$$\text{Ele}[h, f, E^T] = \epsilon^2 \text{Re} E_b \left(\frac{1}{48} h^2 E_t^T + \frac{19}{336} h E^T f_x + \frac{5}{112} f E^T h_x + \frac{15}{224} f h E_x^T \right). \quad (69)$$

In order to cope with the term E_t^T we note that

$$\frac{\partial E^T}{\partial t} = \frac{\partial E^T}{\partial h} \frac{\partial h}{\partial t} + O(\epsilon) = -h^2 h_x \frac{\partial E^T}{\partial h} + O(\epsilon) = -h^2 \frac{\partial E^T}{\partial x} + O(\epsilon). \quad (70)$$

Then we can write

$$\begin{aligned} \text{Ele}[h, f, E^T] &= \frac{\epsilon^2 \text{Re} E_b}{672} (20h^3 h_x E^T + h^4 E_x^T) + O(\epsilon^3) \\ &= \epsilon^2 \text{Re} E_b \left(\frac{5}{56} f h_x E^T + \frac{1}{224} f h E_x^T \right) + O(\epsilon^3). \quad (71) \end{aligned}$$

5. Regularized reduced model

The system (67) and (68) represents a reduced model. However, it is expected to suffer from unphysical blowup due to the effect of the highly nonlinear terms in $\text{Ine}[h, f]$ [22]. Similarly, the high order of the nonlinearities in the second-order electrostatic terms in $\text{Ele}[h, f, E^T]$ (71) risks them violating the assumption that they are asymptotically smaller than the first-order terms as seen in an analogous thermal situation by Scheid *et al.* [32] (and indeed there the relevant terms were identified as the cause of unphysical behavior of the governing equations). We therefore pursue the standard regularization procedure [22,32]. We consider the inertial part of the residuals, the rest of the formula being contained in the term \mathcal{F} , thus

$$\epsilon \text{Re} \left[\overbrace{f_t + \frac{17}{7} \frac{f}{h} f_x - \frac{9}{7} \frac{f^2}{h^2} h_x}^{\mathcal{R}_0^{(1), \text{Re}}} \right] + \epsilon^2 \text{Re} \left[\overbrace{\frac{h^7 h_x^2}{630} - E_b \left(\frac{5}{56} f h_x E^T + \frac{1}{224} f h E_x^T \right)}^{\mathcal{R}_0^{(2), \text{Re}}} \right] = \mathcal{F}. \quad (72)$$

This is rewritten as $\epsilon \mathcal{R}_0^{(1),\text{Re}} + \epsilon^2 \mathcal{R}_0^{(2),\text{Re}} = \mathcal{G}(\epsilon \mathcal{R}_0^{(1),\text{Re}})$, so that the system may be re-expressed as $\epsilon \mathcal{R}_0^{(1),\text{Re}} = \mathcal{G}^{-1} \mathcal{F}$. Using first-order equivalences, this suggests

$$\mathcal{G} = 1 + \epsilon \frac{\mathcal{R}_0^{(1),\text{Re}}}{\mathcal{R}_0^{(2),\text{Re}}} \quad (73)$$

$$\begin{aligned} &= 1 + \epsilon \frac{\frac{h^7 h_x^2}{630} - E_b \left(\frac{5}{56} f h_x E^T + \frac{1}{224} f h E_x^T \right)}{-\frac{1}{3} h^4 h_x} + O(\epsilon^2) \\ &= 1 + \epsilon \left[-\frac{f h_x}{70} + E_b \left(\frac{5}{56} \frac{E^T}{h} + \frac{1}{224} \frac{E_x^T}{h_x} \right) \right] + O(\epsilon^2). \end{aligned} \quad (74)$$

Note, however, that while h can never be 0 (as we do not consider exact touchdown), h_x can (and indeed must on periodic domains) attain a value of 0. Thus the term $\frac{E_x^T}{h_x}$ is not in fact included in the regularization procedure. Thus we are led to the equation

$$\begin{aligned} \epsilon \text{Re } f_t &= \epsilon \text{Re} \left(\frac{9}{7} \frac{f^2}{h^2} h_x - \frac{17}{7} \frac{f}{h} f_x \right) + \left\{ 1 + \epsilon \left(-\frac{f h_x}{70} + E_b \frac{5}{56} \frac{E^T}{h} \right) \right\}^{-1} \\ &\quad \times \left[\frac{5}{6} h - \frac{5}{2} \frac{f}{h^2} + \epsilon \left(\frac{5}{6} \frac{h_{xxx} h}{\text{Ca}} + \frac{5}{6} E_b h E_x^N - \frac{5}{4} E_b E^T \right) \right] \\ &\quad + \epsilon^2 \left(4 \frac{f}{h^2} h_x^2 + \frac{9}{2} f_{xx} - \frac{9}{2} \frac{1}{h} f_x h_x - 6 \frac{f}{h} h_{xx} \right) + \epsilon^2 \frac{\text{Re } E_b}{224} f h E_x^T. \end{aligned} \quad (75)$$

This is relatively simple to validate: the hydrodynamic portion of the model here only differs from the electrostatically passive case of Scheid *et al.* [22] by virtue of the incorporation of additional stress at the interface, both normal and tangential. Although the stress is from a different source, this is analogous to the situation of Scheid *et al.* [32], to which our model may be compared under the replacement of the tangential stress term $\mathcal{M} \partial_x \theta \leftrightarrow E_b E^T$, and the incorporation of the normal stress $h_{xxx} \rightarrow h_{xxx} + E_b E_x^N$.

We note that Scheid *et al.* [22] see little to no numerical advantage to using the regularized model over simply neglecting the second-order inertial effects. This is interesting as, unlike the regularized model, this is no longer accurate at second order for Reynolds numbers of order unity. Thus for comparison we also consider the *simplified* model

$$\begin{aligned} \epsilon \text{Re } f_t &= \epsilon \text{Re} \left(\frac{9}{7} \frac{f^2}{h^2} h_x - \frac{17}{7} \frac{f}{h} f_x \right) + \left[\frac{5}{6} h - \frac{5}{2} \frac{f}{h^2} + \epsilon \left(\frac{5}{6} \frac{h_{xxx} h}{\text{Ca}} + \frac{5}{6} E_b h E_x^N - \frac{5}{4} E_b E^T \right) \right] \\ &\quad + \epsilon^2 \left(4 \frac{f}{h^2} h_x^2 + \frac{9}{2} f_{xx} - \frac{9}{2} \frac{1}{h} f_x h_x - 6 \frac{f}{h} h_{xx} \right). \end{aligned} \quad (76)$$

This model does, however, retain the second-order viscous dispersion effects, as given on the second line, which cause a wave number dependence of wave speeds. This has been noted as being particularly important for the prediction of capillary ripples, which is crucial to pulse interaction theories [33].

IV. TWO-DIMENSIONAL VALIDATION

A. Validation using linear stability analysis

1. Exact linear solution

Introduction of a stream function and linearization gives an Orr-Sommerfeld system

$$\text{Re}(ikU + \sigma)(d_y^2 - k^2)\psi - \text{Re } U_{yy} ik\psi = (d_y^2 - k^2)^2 \psi, \quad (77)$$

where $u = U + \delta \tilde{u}$, $v = \delta \tilde{v}$, with $(\tilde{u}, \tilde{v}) = (\psi_y, -ik\psi) \exp(\sigma t + ikx)$.

The perturbations to the electrostatic potentials are governed by

$$\tilde{\phi}_{yy}^{A,F} - k^2 \tilde{\phi}^{A,F} = 0, \quad \tilde{\phi}^F|_0 = 0, \quad \tilde{\phi}^A|_d = 0,$$

which gives

$$\tilde{\phi}^F = \tilde{c}_F \sinh(ky), \quad \tilde{\phi}^A = \tilde{c}_A \sinh[k(y-d)]. \quad (78)$$

The continuity (9) and Gauss (10) conditions expanded about $h = 1 + \delta\tilde{h}$ give

$$\frac{(\Sigma_A - \Sigma_F)}{\Sigma_A - \Sigma_F(1-d)} \tilde{h} + \tilde{c}_F \sinh(k) = \tilde{c}_A \sinh[k(1-d)], \quad (79)$$

$$-\tilde{q} = \epsilon_A \tilde{c}_A k \cosh[k(1-d)] - \epsilon_F \tilde{c}_F k \cosh(k), \quad (80)$$

respectively. Linearization of (11) and decomposition into normal modes results in

$$(\sigma + ikU)\tilde{q} + ik\tilde{q}(U_y\tilde{h} + \psi_y) = \Sigma_A \tilde{c}_A k \cosh[k(1-d)] - \Sigma_F \tilde{c}_F k \cosh(k), \quad (81)$$

while the kinematic, no-slip, and impermeability conditions become

$$(\sigma + ikU)\tilde{h} = -ik\psi, \quad \psi(1) = \psi'(1) = 0. \quad (82)$$

The normal (5) and tangential (6) stress conditions become

$$\begin{aligned} & \frac{i}{k} \{k^2 \psi_y - \psi_{yyy} + \text{Re}[(\sigma + ikU)\psi_y - ikU_y \psi]\} \\ & = \frac{k^2 \tilde{h}}{\text{Ca}} + 2(-ik\psi_y - ik\tilde{h}U_y)E_b [\epsilon_A (\tilde{\phi}_y^A \tilde{\phi}_y^A) - \epsilon_F (\tilde{\phi}_y^F \tilde{\phi}_y^F)], \end{aligned} \quad (83)$$

$$U_{yy}\tilde{h} + \psi_{yy} + k^2\psi = -\tilde{q} [ik\tilde{c}_F \sinh(k) + ik\tilde{h}\tilde{\phi}_y^F]. \quad (84)$$

We thus have a fourth order ODE for ψ (77) plus four additional unknowns, \tilde{c}_A , \tilde{c}_F , \tilde{h} , and \tilde{q} . Thus eight boundary conditions are required; these are given by (79)–(84). This is thus a closed problem which is solved using the Chebyshev-Tau algorithm.

2. Weighted residual, leading-order electrostatics

In order to linearize the regularized model (36) and (75) with the leading-order expressions for the electric fields (29) and (30), we set $h = 1 + \epsilon\tilde{h}e^{\sigma t + ikz}$, $q = \frac{1}{3} + \epsilon\tilde{q}e^{\sigma t + ikz}$. Then we find that

$$\begin{aligned} \left\{ \text{Re} \sigma + \frac{9}{2}k^2 + i\text{Re} \frac{17}{21}k + \frac{5}{2} \right\} \tilde{q} &= \frac{5}{2} - i \frac{1}{\text{Ca}} \frac{5}{6}k^3 + 2k^2 + i \text{Re} \frac{1}{7}k + i E_b \frac{5}{6} \frac{(\sigma_R - 1)(\epsilon_A \sigma_R^2 - \epsilon_F)}{[1 + \sigma_R(d-1)]^3} k \\ &+ E_b \frac{d(840i + \text{Re}k)\sigma_R(\epsilon_A \sigma_R - \epsilon_F)}{672[1 + \sigma_R(d-1)]^3} k \left\} \tilde{h}, \end{aligned} \quad (85)$$

$$\sigma \tilde{h} + ik\tilde{q} = 0, \quad (86)$$

where the two electrostatic terms, multiplied by E_b , correspond to the normal and tangential components of the electrostatic stress, respectively.

3. Weighted residual, second-order electrostatics

In order to linearize the regularized second-order electrostatic model (36) and (75) with the full second-order form for the electric fields (23) and (32)–(34), we set

$$(h, q, c_F, c_A) = \left(1, \frac{1}{3}, \frac{1}{1 + \sigma_R(d-1)}, \frac{\sigma_R}{1 + \sigma_R(d-1)} \right) + \epsilon(\tilde{h}, \tilde{q}, \tilde{c}_F, \tilde{c}_A)e^{\sigma t + ikz}. \quad (87)$$

Linearization gives the matrix problem in Appendix A.

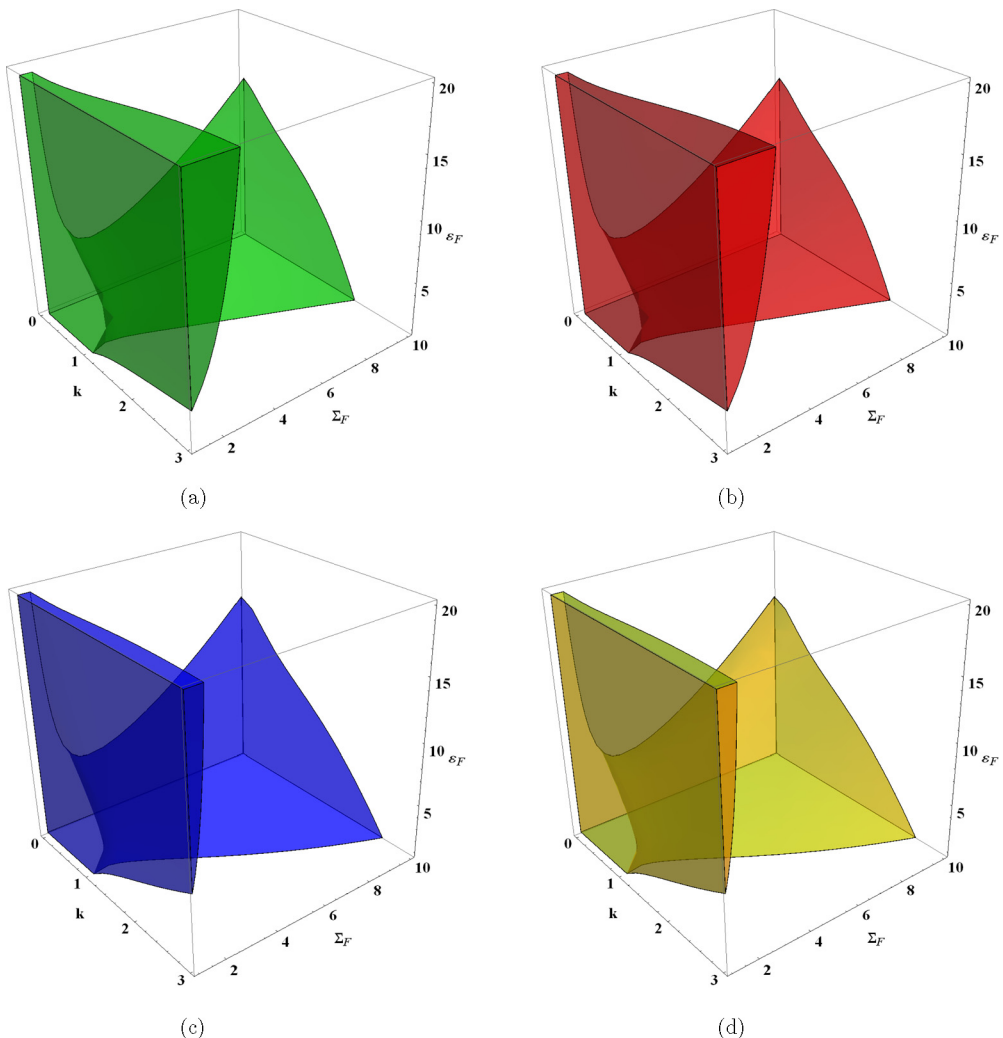


FIG. 2. Comparison of the predictions of linear stability for $\text{Re} = 5, d = 2, E_b = 2$. Neutral stability surfaces are plotted according to (a) Orr-Sommerfeld with full charge evolution equation, (b) Orr-Sommerfeld with high conductivity approximation, (c) regularized model—leading-order electrostatics: (36), (75), (29), and (30), (d) regularized model—full second-order electrostatics: (36), (75), (23), and (32)–(34).

4. Linear stability comparison

We compare the linear stability calculations in Secs. IV A 2 and IV A 3 to two variants of the Orr-Sommerfeld calculations: one where we have used the full linearized form of the charge evolution equation (81), and one where we have taken the high conductivity limit by neglecting the left-hand-side of this equation. In the former case we have taken $\Sigma_A = 10^6, \Sigma_F = \sigma_R \times \Sigma_A$ to emulate high conductivities of the correct ratio. The results are given in Fig. 2. The two Orr-Sommerfeld calculations (a) and (b) of course agree exceptionally well. This is as expected as the left-hand-side of (11) is negligible for large conductivities. In combination with previous numerical evidence [17,30] we now make exclusive use of the high conductivity approximation, neglecting the left-hand-side of (20) as in Sec. III A.

The agreement between the Orr-Sommerfeld solutions and the weighted residual solutions is quite strong in large regions of parameter space, especially where the disturbances lie in the

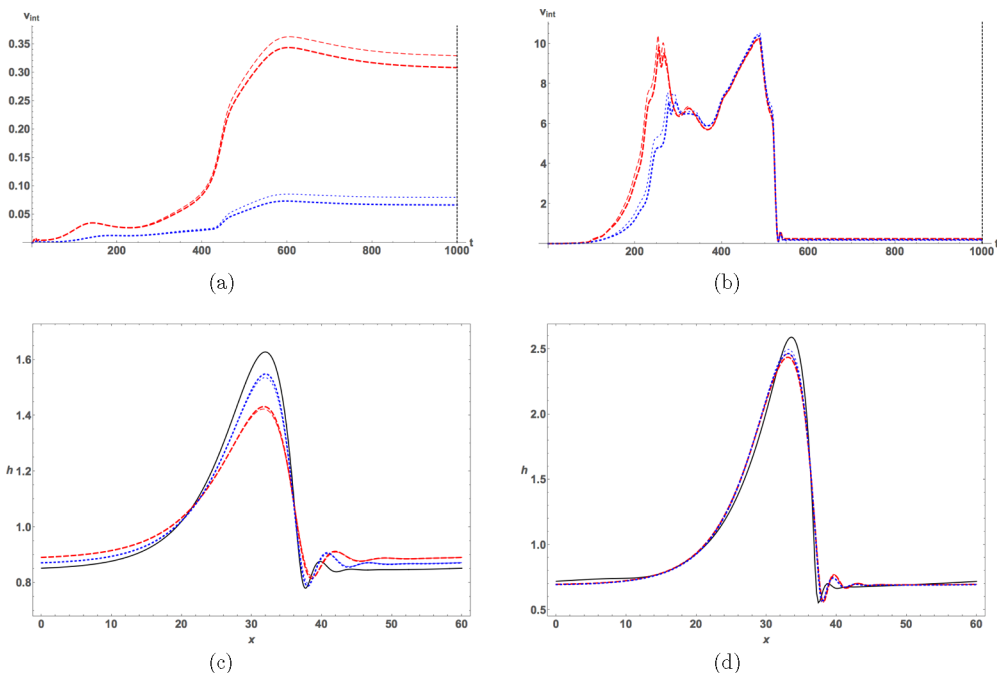


FIG. 3. Comparison of the nonlinear predictions of the different models for $\text{Re} = 15, \text{Ca} = 0.1, d = 6, \epsilon_A = 1, E_b = 30, L = 60$. Top: integral square difference of the interfacial shapes $v_{\text{int}}(h_1, h_2)$ (88); bottom: interface shapes at $t = 1000$. (a), (c): $\epsilon_F = 2, \sigma_R = 0.5$; (b), (d): $\epsilon_F = 0.5, \sigma_R = 2$, solid thick line: DNS, thin lines: regularized models, thick lines: simplified models, dotted lines: second-order electrostatics (32)–(34), dashed lines: first-order electrostatics (29) and (30).

long-wave regime. However, for example, for $\Sigma_F \sim 2$ and $\epsilon_F > 10$ we find that the range of unstable wave numbers is exclusively in the region $k > 1$ for the Orr-Sommerfeld calculations (a) and (b). Unsurprisingly, in this situation, these models, which are based on long-wave approximations, do not provide such accurate agreement, as seen in panels (c) and (d).

B. Validation via nonlinear direct numerical simulations

1. Transient comparison of interfacial shapes

We perform time-dependent computations of the different models, all on periodic domains with centered finite differences in space. Direct numerical simulations are performed by rescaling the computational domains of both phases into rectangles. For the lower liquid region the rescaling $Y = y/h$ is used, while for the upper gas region the rescaling $Z = (y - h)/(d - h)$ so that $0 \leq Y, Z \leq 1$. An implicit second-order Newton-Raphson time-stepping method is used to simultaneously solve the coupled equations for the electric fields, the fluid velocities, and the pressure in the liquid region, as well as for the electric field in the gas region. The regularized (75) and simplified (76) models are solved, both for the leading-order electrostatic model (29) and (30), and for the second-order electrostatics (23) and (32)–(34). For the leading-order electrostatic models the electric fields are known as explicit functions of the interfacial shape h , and so an explicit Runge-Kutta-45 solver is used. For the second-order methods the fields are only known implicitly, and so an implicit solver using the trapezoidal rule in time is used. All simulations have been compared against linear theory providing excellent agreement. Mesh and time-step refinement have been checked to ensure convergence.

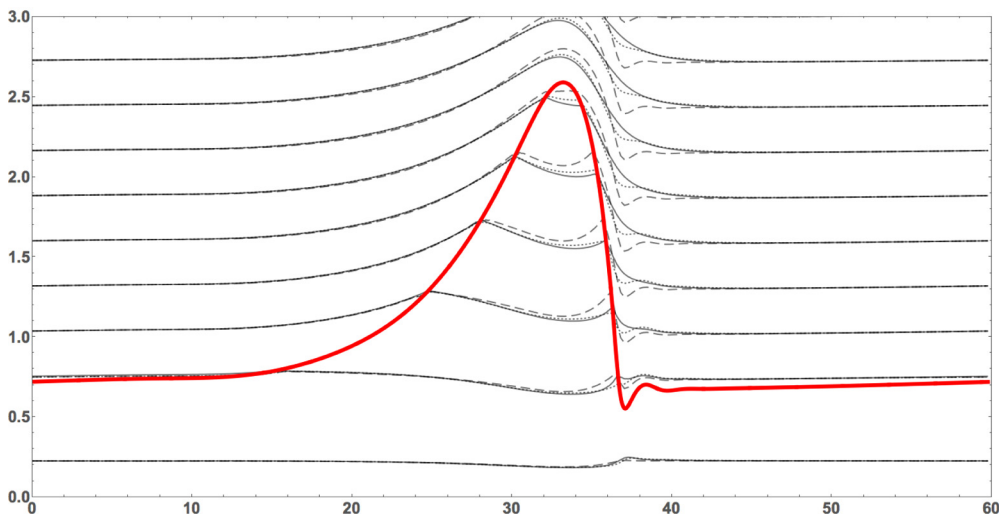


FIG. 4. Comparison of computed equipotential lines for $\text{Re} = 15, \text{Ca} = 0.1, d = 6, \epsilon_A = 1, \epsilon_F = 0.5, \sigma_R = 2, E_b = 30$. Thick line: interfacial shape extracted from direct numerical simulation for right-hand case of Fig. 3. Thin, solid line: full solution as given by direct numerical simulations; thin dashed line: leading-order model (29) and (30); thin dotted line: second-order model (32)–(34). Lines plotted correspond to equipotentials of $\phi = 0.02, 0.07, 0.12, \dots, 0.97$. While the upper electrode is at $y = 6$ we only plot up to $y = 3$, with an upper equipotential of $\phi = 0.57$.

In order to compare the output of the respective models, we use the metric

$$v_{\text{int}}(h_1, h_2) = \min_{x_c} \int_0^L |h_1(x) - h_2(x + x_c)|^2 dx, \quad (88)$$

where $x_c \in [0, L)$ and the domain is periodic, and h_1 and h_2 are the interfacial shapes we wish to compare. This is the integral square difference minimised over periodic translation, chosen because it reflects the level of agreement between interfacial shapes, in which we are predominantly interested. Interpolation is used to ensure subgridpoint matching accuracy.

We compare each reduced order model to the output of the direct numerical simulations using $v_{\text{int}}(h_i, h_{\text{DNS}})$ in Fig. 3, where h_i is the interfacial shape of each low-order model, and h_{DNS} is the output of the direct numerical simulations. Previous studies [19,30] have shown that the critical governing parameters for the stability of the system are the ratios of the permittivities and conductivities. We therefore choose a representative set of parameters where inertia is important ($\text{Re} = 15$) and surface tension is significant ($\text{Ca} = 0.1$), but where the effect of the electric fields should be at least as strong as either of these effects ($E_b = 30$). We then fix $\epsilon_A = 1$ so that varying ϵ_F is effectively changing the permittivity ratio, and select parameter sets from two opposite sides of the range, where $\epsilon_F = 2$ and $\sigma_R = 0.5$, and where $\epsilon_F = 0.5$ and $\sigma_R = 2$. The distance of the outer electrode $d = 6$ has been chosen primarily to be outside the typical heights of the observed waves; we will investigate it in more detail in Sec. V. We find that in fact the simplified models provide better accuracy than the regularized models. This may initially seem surprising as the regularized model is formally second-order accurate, whereas the simplified model is not. However, the regularization procedure is somewhat *ad hoc*. Furthermore, this finding is in line with those of Scheid *et al.* [22]. This is significant as the majority of the derivations in Secs. III B 3–III B 5 become superfluous if one only wishes to derive the simplified model [34], dramatically simplifying the process.

We also find that the second-order electrostatic solutions typically provide better agreement, and indeed we investigate this in more detail in Sec. IV B 2. However, the cost of solving the additional boundary value problem is likely to be prohibitive, especially in three dimensions. We also note

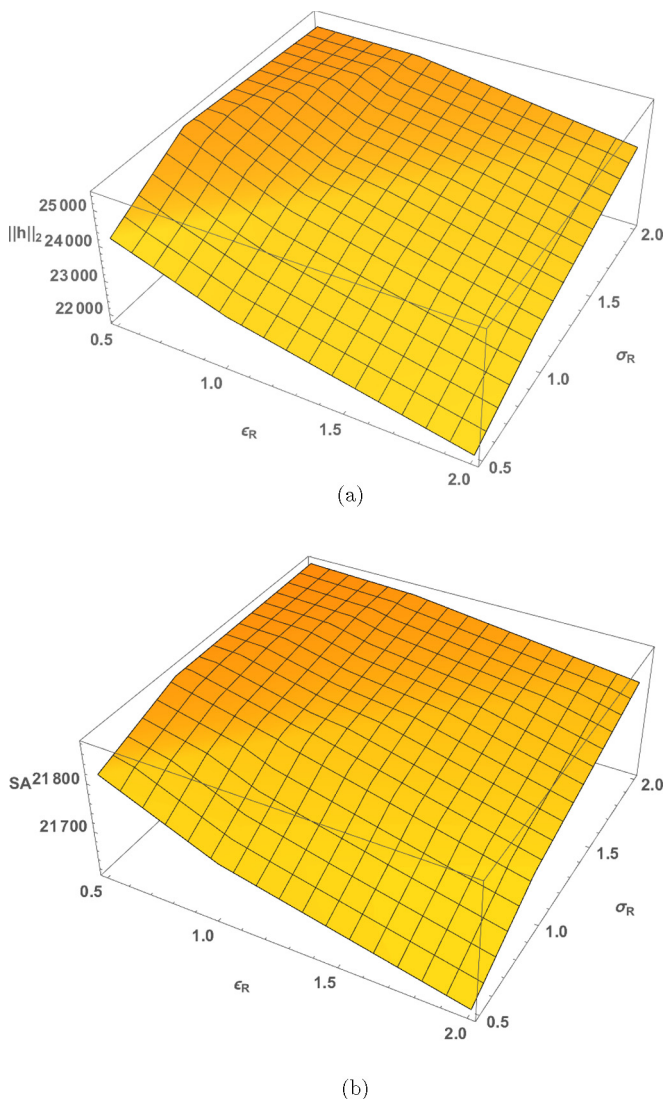


FIG. 5. Results of a three-dimensional parametric study with $Re = 15, Ca = 0.1, d = 6, \epsilon_A = 1, E_b = 30$. Variation of $\|h\|_2$ and surface area with ϵ_F and σ_R are shown in (a) and (b), respectively.

that, even in the left-hand figure where the second-order electrostatic model appears to perform significantly better, the absolute value of v_{int} is still actually rather small: the solution is quite accurate. We therefore elect to use the simplified model with the leading-order electrostatics for our three-dimensional computations in Sec. V.

2. Comparison of predicted electrostatic potentials

We wish to compare the accuracy of the potential fields predicted by the leading-order (29) and (30) and second-order (32)–(34) theories. In the high conductivity limit, these are functions purely of the interfacial position h . Therefore, we take the traveling wave produced by the direct numerical simulations for $\epsilon_F = 0.5, \sigma_R = 2$ in the previous section and use this to compute potential fields.

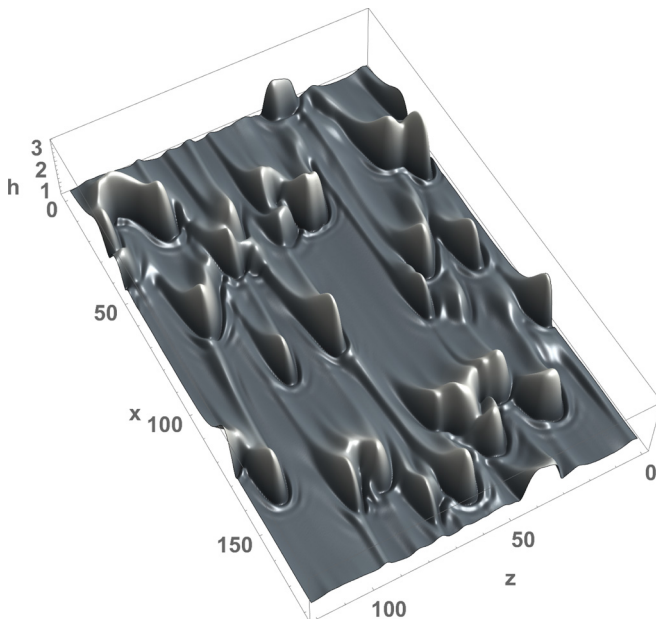


FIG. 6. Surface plot of the interface computed through a transient, three-dimensional simulation with $Re = 15, Ca = 0.1, d = 6, \epsilon_A = 1, E_b = 30, \epsilon_R = 0.5, \sigma_R = 2$, and $t = 500$.

This profile is chosen as it contains the largest gradients of the interfaces produced and will provide the stiffest test of the low-order models. The results are plotted in Fig. 4.

As expected, all models demonstrate a discontinuous jump in gradients at the interface due to the charge accumulated there (10). Away from the peak and capillary ripples all the methods agree quite well. However, in these regions where the gradients are the steepest, it is noticeable that the second-order method (dotted line) provides better agreement with the direct numerical solution (solid line).

Of particular note is the behavior very close to the capillary ripples themselves. For the direct numerical simulation of the full Laplace equation the oscillations exhibited by the interface are only mirrored in the equipotentials exceptionally close to the interface; farther away the equipotentials are monotonic in the gas regions (up to the peak of the wave). This behavior is imitated somewhat by the second-order solution, but the leading-order solution exhibits oscillations throughout the domain.

V. THREE-DIMENSIONAL PARAMETRIC STUDY

The simplicity, accuracy, and speed of computation of the simplified model with the leading-order electrostatics (36), (76), (29), and (30) allows us to perform large-scale numerical computations to discern the fully nonlinear behavior of fluids under the effect of electric fields. Therefore, we extend the simplified model (76) together with the leading-order electrostatics (29) and (30) to three dimensions in the natural way, as in Scheid *et al.* [22] or Scheid *et al.* [32]. We give the equations in Appendix B. This is then computed using a standard Runge-Kutta-45 solver in time together with centered finite differences on a doubly periodic domain in space. The mesh and temporal error parameters were varied to ensure convergence. Comparisons with linear theory and the one-dimensional models were used for validation. We compute both the two-norm and the total surface area, respectively

$$\|h\|_2 = \iint h^2 dx dz, \quad SA = \iint \sqrt{1 + h_x^2 + h_z^2} dx dz. \quad (89)$$

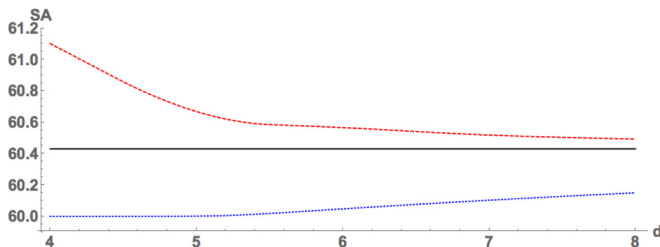


FIG. 7. Surface area variation with electrode distance $4 \leq d \leq 8$. $\text{Re} = 15, \text{Ca} = 0.1, d = 6, \epsilon_A = 1, E_b = 30$. Upper line, dashed: $\epsilon_F = 0.5, \sigma_R = 2$; lower line, dotted: $\epsilon_F = 2, \sigma_R = 0.5$.

We seed the initial state with small amplitude random noise for a variety of values of ϵ_F and σ_R and average these values over three runs up to $t = 500$. The resultant values are plotted in Fig. 5.

We find that increasing the conductivity ratio but decreasing the permittivity ratio results in an increase in both the two-norm and the surface area, generally corresponding to a more disordered interface. We give an example of such an interface in Fig. 6. The surface area of this represents an increase of 1.4% over that of the flat state; this is a 39.5% greater increase in surface area than is encountered in the electrostatically passive case. The magnitude of this increase is unsurprising; asserting the expected order of the gradients gives $\iint \sqrt{1 + \epsilon^2 h_x^2 + \epsilon^2 h_z^2} dx dz = \iint 1 dx dz + O(\epsilon^2)$.

The final parameter which we have not considered is the distance of the outer electrode d . Physically, we anticipate with a reduced value of d , giving the same potential drop across a shorter distance and thus a greater electric field strength, will result in an accentuation of the observed physical behaviors. This corroborates the predictions of both linear and nonlinear theories. For simplicity consider the simplified model with leading-order electrostatics (76), (29), and (30). We find that d enters these equations solely via its contributions to the denominators in Eq. (29). Thus we find that

$$E_b E^N = \frac{E_b}{[h - \sigma_R(h - d)]^2} t_1(x, t), \quad (90)$$

$$E_b E^T = \frac{E_b}{[h - \sigma_R(h - d)]^2} \left[h_x - \frac{h_x(1 - \sigma_R)}{h - \sigma_R(h - d)} \right] t_2(x, t), \quad (91)$$

where t_1 and t_2 are independent of d . These forms are in line with our physical inferences: for increasing d we have that $E_b E^N \sim E_b/d^2$, $E_b E^T \sim E_b/d^3$, so that the effect of the electric fields is effectively weaker. We note, however, that for sufficiently large values of d , corresponding to the outer electrode being far away, the slenderness approximation in the gas phase is no longer valid, and thus this inference should be treated with caution.

In order to test this, we again take our characteristic values of $\epsilon_F = 0.5, \sigma_R = 2$ and $\epsilon_F = 2, \sigma_R = 0.5$ as characteristic destabilizing and stabilizing cases, respectively. We then compute the arc length at $t = 1000$ for $4 \leq d \leq 8$ for two-dimensional computations. The results are plotted in Fig. 7. As anticipated, a lower value of d accentuates the effect that the electric field is having, be that stabilizing or destabilizing.

VI. CONCLUSIONS

The behavior of a film falling down a vertical wall in the presence of an electric field has been investigated. An asymptotic long-wave expansion combined with the method of weighted residuals has been used to derive multiple models for the flow. The hydrodynamic component of the problem has been reduced to two sets of model equations. One model corresponds to a simplified model, neglecting second-order inertial effects. The other model was derived using a reduction and

regularization procedure on the full five-equation second-order model to derive another two-equation model, which is fully consistent at second order. We have also shown that a similar separation of variables approach can be applied to the electrostatic problem, both at leading order and at second order.

Comparisons with direct numerical simulations have shown that, despite the additional effort involved, the regularized model is inferior to the simplified model by the metric defined in the present work. The second-order electrostatic model has been shown to be more accurate, although the leading-order model is satisfactory and offers substantial gains in terms of computational cost. The resultant high-speed, high-accuracy simplified model together with the leading-order electrostatic solution has been used to perform a parametric study of the three-dimensional problem. This has shown that increasing the conductivity ratio and decreasing the permittivity ratio results in a more disordered interface, corresponding to an increase in both the two-norm and the total surface area.

ACKNOWLEDGMENTS

The authors thank the Engineering and Physical Sciences Research Council, UK, for their support through the MEMPHIS Programme Grant (EP/K003976/1), the MACIPh Platform Grant (EP/L020564/1), as well as EPSRC Grant EP/K041134/1 to DTP, and a Doctoral Prize Fellowship for AWW.

APPENDIX A: REGULARIZED SECOND-ORDER ELECTROSTATIC LINEARIZATION

The linear stability problem can be posed as a matrix problem

$$A \begin{pmatrix} \tilde{h} \\ \tilde{q} \\ \tilde{c}_F \\ \tilde{c}_A \end{pmatrix} = 0, \quad (\text{A1})$$

where

$$A = \begin{pmatrix} \sigma & ik & 0 & 0 \\ \frac{5}{2} + i\frac{\text{Re}k}{7} + 2\eta k^2 - i\frac{5}{6}\frac{k^2}{\text{Ca}} + q_h & -\frac{5}{2} - i\text{Re}\frac{17}{21}k - \frac{9}{2}\eta k^2 - \text{Re}\sigma & q_F & q_A \\ \frac{1-\sigma_R}{1+\sigma_R(d-1)} & 0 & \frac{1}{6}(6+k^2) & C_A \\ 0 & 0 & \frac{1}{2}(2+k^2)\sigma_R & U_A \end{pmatrix}, \quad (\text{A2})$$

where

$$q_h = \frac{(840i + \text{Re}k)(\epsilon_A\sigma_R - \epsilon_F)}{672(1 + \sigma_R(d-1))^2}, \quad (\text{A3})$$

$$q_F = -iE_b\epsilon_F \frac{5}{12} \frac{(2+k^2)}{1 + \sigma_R(d-1)} - E_b \frac{(840i + \text{Re}k)(6+k^2)(\epsilon_F - \epsilon_A\sigma_R)}{4032[1 + \sigma_R(d-1)]}, \quad (\text{A4})$$

$$q_A = iE_b\epsilon_A\sigma_R \frac{5}{12} \frac{[2 + (d-1)^2k^2]}{12[1 + \sigma_R(d-1)]}, \quad (\text{A5})$$

$$C_A = \frac{1}{6}(d-1)[6 + (d-1)^2k^2], \quad (\text{A6})$$

$$U_A = -1 - \frac{1}{2}(d-1)^2k^2. \quad (\text{A7})$$

APPENDIX B: SIMPLIFIED THREE-DIMENSIONAL EQUATIONS

$$h_t = -f_x - g_z, \quad (\text{B1})$$

$$\text{Re } f_t = -\frac{5}{2} \frac{f}{h^2} + \frac{5}{6} h \quad (\text{B2})$$

$$+ \frac{5}{6} h \frac{h_{xxx} + h_{zzz}}{\text{Ca}} + \frac{5}{6} h E_b E_x^N - \frac{5}{4} E_b E^T \quad (\text{B3})$$

$$+ \text{Re} \left[\frac{9}{7} \frac{f^2 h_x}{h^2} - \frac{17}{7} \frac{f f_x}{h} - \frac{8}{7} \frac{f g_z}{h} - \frac{9}{7} \frac{g f_z}{h} + \frac{9}{7} \frac{f g h_z}{h^2} \right] \quad (\text{B4})$$

$$+ 4 \frac{f h_x^2}{h^2} - \frac{9}{2} \frac{f_x h_x}{h} - 6 \frac{f h_{xx}}{h} + \frac{9}{2} f_{xx} + \frac{13}{4} \frac{g h_x h_z}{h^2} - \frac{f_z h_z}{h} - \frac{43}{16} \frac{g_x h_z}{h} \quad (\text{B5})$$

$$- \frac{13}{16} \frac{g_z h_x}{h} + \frac{3}{4} \frac{f h_z^2}{h^2} - \frac{23}{16} \frac{f h_{zz}}{h} - \frac{73}{16} \frac{g h_{xz}}{h} + f_{zz} + \frac{7}{2} g_{xz}, \quad (\text{B6})$$

$$\text{Re } g_t = -\frac{5}{2} \frac{g}{h^2} \quad (\text{B7})$$

$$+ \frac{5}{6} h \frac{h_{xzz} + h_{zzz}}{\text{Ca}} + \frac{5}{6} h E_b E_z^N - \frac{5}{4} E_b E_\perp^T \quad (\text{B8})$$

$$+ \text{Re} \left[\frac{9}{7} \frac{g^2 h_z}{h^2} - \frac{17}{7} \frac{g g_z}{h} - \frac{8}{7} \frac{g f_x}{h} - \frac{9}{7} \frac{f g_x}{h} + \frac{9}{7} \frac{f g h_x}{h^2} \right] \quad (\text{B9})$$

$$+ 4 \frac{g h_z^2}{h^2} - \frac{9}{2} \frac{g_z h_z}{h} - 6 \frac{g h_{zz}}{h} + \frac{9}{2} g_{zz} + \frac{13}{4} \frac{f h_x h_z}{h^2} - \frac{h_z g_z}{h} - \frac{43}{16} \frac{f_z h_x}{h} \quad (\text{B10})$$

$$- \frac{13}{16} \frac{f_x h_z}{h} + \frac{3}{4} \frac{g h_x^2}{h^2} - \frac{23}{16} \frac{g h_{xx}}{h} - \frac{73}{16} \frac{f h_{xz}}{h} + g_{zz} + \frac{7}{2} f_{xz}, \quad (\text{B11})$$

$$E_\perp^T = q(c_F h)_z. \quad (\text{B12})$$

-
- [1] J. Darabi, M. M. Ohadi, and S. V. Desiatoun, Falling film and spray evaporation enhancement using an applied electric field, *J. Heat Transfer* **122**, 741 (2000).
- [2] J. Darabi, M. M. Ohadi, and S. V. Dessiatoun, Augmentation of thin falling-film evaporation on horizontal tubes using an applied electric field, *J. Heat Transfer* **122**, 391 (2000).
- [3] M. N. Pantzali, A. A. Mouza, and S. V. Paras, Counter-current gas-liquid flow and incipient flooding in inclined small diameter tubes, *Chem. Eng. Sci.* **63**, 3966 (2008).
- [4] D. Tseluiko and S. Kalliadasis, Nonlinear waves in counter-current gas-liquid film flow, *J. Fluid Mech.* **673**, 19 (2011).
- [5] R. V. Craster and O. K. Matar, Dynamics and stability of thin liquid films, *Rev. Mod. Phys.* **81**, 1131 (2009).
- [6] A. Oron, S. H. Davis, and S. G. Bankoff, Long-scale evolution of thin liquid films, *Rev. Mod. Phys.* **69**, 931 (1997).
- [7] P.-G. De Gennes, Wetting: Statics and dynamics, *Rev. Mod. Phys.* **57**, 827 (1985).
- [8] R. D. Deegan, O. Bakajin, T. F. Dupont, G. Huber, S. R. Nagel, and T. A. Witten, Capillary flow as the cause of ring stains from dried liquid drops, *Nature (London)* **389**, 827 (1997).

- [9] H. B. Eral, D. M. Augustine, M. H. G. Duits, and F. Mugele, Suppressing the coffee stain effect: How to control colloidal self-assembly in evaporating drops using electrowetting, *Soft Matter* **7**, 4954 (2011).
- [10] D. A. Saville, Electrohydrodynamics: The Taylor-Melcher leaky dielectric model, *Annu. Rev. Fluid Mech.* **29**, 27 (1997).
- [11] R. S. Allan and S. G. Mason, Particle behavior in shear and electric fields. I. Deformation and burst of fluid drops, *Proc. Roy. Soc. London A* **267**, 45 (1962).
- [12] L. F. Pease III and W. B. Russel, Linear stability analysis of thin leaky dielectric films subjected to electric fields, *J. Non-Newtonian Fluid Mech.* **102**, 233 (2002).
- [13] V. Shankar and A. Sharma, Instability of the interface between thin fluid films subjected to electric fields, *J. Colloid Interface Sci.* **274**, 294 (2004).
- [14] D. Bandyopadhyay and A. Sharma, Electric field induced instabilities in thin confined bilayers, *J. Colloid Interface Sci.* **311**, 595 (2007).
- [15] R. Verma, A. Sharma, K. Kargupta, and J. Bhaumik, Electric field induced instability and pattern formation in thin liquid films, *Langmuir* **21**, 3710 (2005).
- [16] D. Tseluiko and D. T. Papageorgiou, Dynamics of an electrostatically modified Kuramoto–Sivashinsky–Korteweg–de Vries equation arising in falling film flows, *Phys. Rev. E* **82**, 016322 (2010).
- [17] R. V. Craster and O. K. Matar, Electrically induced pattern formation in thin leaky dielectric films, *Phys. Fluids* **17**, 032104 (2005).
- [18] A. Corbett and S. Kumar, Spreading of thin droplets of perfect and leaky dielectric liquids on inclined surfaces, *Langmuir* **32**, 6606 (2016).
- [19] O. Ozen, D. T. Papageorgiou, and P. G. Petropoulos, Nonlinear stability of a charged electrified viscous liquid sheet under the action of a horizontal electric field, *Phys. Fluids* **18**, 042102 (2006).
- [20] D. Tseluiko and D. T. Papageorgiou, Wave evolution on electrified falling films, *J. Fluid Mech.* **556**, 361 (2006).
- [21] O. Ozen, N. Aubry, D. T. Papageorgiou, and P. G. Petropoulos, Electrohydrodynamic linear stability of two immiscible fluids in channel flow, *Electrochim. Acta* **51**, 5316 (2006).
- [22] B. Scheid, C. Ruyer-Quil, and P. Manneville, Wave patterns in film flows: Modeling and three-dimensional waves, *J. Fluid Mech.* **562**, 183 (2006).
- [23] D. J. Benney, Long waves on liquid films, *J. Math. Phys.* **45**, 150 (1966).
- [24] A. Pumir, P. Manneville, and Y. Pomeau, On solitary waves running down an inclined plane, *J. Fluid Mech.* **135**, 27 (1983).
- [25] O. Takeshi, Surface equation of falling film flows with moderate Reynolds number and large but finite Weber number, *Phys. Fluids* **11**, 3247 (1999).
- [26] S. Kalliadasis, C. Ruyer-Quil, B. Scheid, and M. G. Velarde, *Falling Liquid Films*, Applied Mathematical Sciences Vol. 176 (Springer-Verlag, New York, 2012).
- [27] C. Ruyer-Quil and P. Manneville, Improved modeling of flows down inclined planes, *Eur. Phys. J. B* **15**, 357 (2000).
- [28] C. Ruyer-Quil and P. Manneville, Further accuracy and convergence results on the modeling of flows down inclined planes by weighted-residual approximations, *Phys. Fluids* **14**, 170 (2002).
- [29] S. Chakraborty, P.-K. Nguyen, C. Ruyer-Quil, and V. Bontozoglou, Extreme solitary waves on falling liquid films, *J. Fluid Mech.* **745**, 564 (2014).
- [30] A. W. Wray, D. T. Papageorgiou, and O. K. Matar, Electrified coating flows on vertical fibres: Enhancement or suppression of interfacial dynamics, *J. Fluid Mech.* **735**, 427 (2013).
- [31] C. Ruyer-Quil, B. Scheid, S. Kalliadasis, M. G. Velarde, and R. K. Zeytounian, Thermocapillary long waves in a liquid film flow. Part 1. Low-dimensional formulation, *J. Fluid Mech.* **538**, 199 (2005).
- [32] B. Scheid, S. Kalliadasis, C. Ruyer-Quil, and P. Colinet, Interaction of three-dimensional hydrodynamic and thermocapillary instabilities in film flows, *Phys. Rev. E* **78**, 066311 (2008).
- [33] M. Pradas, D. Tseluiko, and S. Kalliadasis, Rigorous coherent-structure theory for falling liquid films: Viscous dispersion effects on bound-state formation and self-organization, *Phys. Fluids* **23**, 044104 (2011).
- [34] C. Ruyer-Quil, P. Treveleyan, F. Giorgiutti-Dauphiné, C. Duprat, and S. Kalliadasis, Modelling film flows down a fibre, *J. Fluid Mech.* **603**, 431 (2008).